HHS Public Access

Author manuscript

Nat Chem Biol. Author manuscript; available in PMC 2020 November 07.

Published in final edited form as:

Nat Chem Biol. 2020 August ; 16(8): 841–849. doi:10.1038/s41589-020-0535-8.

"TRUPATH, an Open-Source Biosensor Platform for Interrogating the GPCR Transducerome"

Reid H.J. Olsen[1,#], **Jeffrey F. DiBerto**[1,#], **Justin G. English**[1], **Alexis M. Glaudin**[1], **Brian E. Krumm**[1], **Samuel T. Slocum**[1,3], **Tao Che**[1], **Ariana C. Gavin**[1], **John D. McCorvy**[1], **Bryan L. Roth**[1,2,3,*], **Ryan T. Strachan**[1,*]

[1]Department of Pharmacology, University of North Carolina Chapel Hill School of Medicine;

[2]Division of Chemical Biology and Medicinal Chemistry, Eshelman School of Pharmacy, University of North Carolina Chapel Hill;

[3]National Institute of Mental Health Psychoactive Drug Screening Program, University of North Carolina Chapel Hill School of Medicine, Chapel Hill, NC 27514

Abstract

G protein-coupled receptors (GPCRs) remain major drug targets despite our incomplete understanding of how they signal through 16 non-visual G protein signal transducers (collectively named the transducerome) to exert their actions. To address this gap, we developed an open-source suite of 14 optimized Bioluminescence Resonance Energy Transfer (BRET) Gαβγ biosensors (dubbed TRUPATH) to interrogate the transducerome with single pathway resolution in cells. Generated through exhaustive protein engineering and empirical testing, the TRUPATH suite of Gαβγ biosensors includes the first Gα15 and GαGustducin probes. In head-to-head studies, TRUPATH biosensors outperformed first-generation sensors at multiple GPCRs and in different cell lines. Benchmarking studies with TRUPATH biosensors recapitulated previously documented signaling bias and revealed new coupling preferences for prototypic and understudied GPCRs with potential *in vivo* relevance. To enable a greater understanding of GPCR molecular pharmacology by the scientific community, we have made TRUPATH biosensors easily accessible as a kit through Addgene.

*Correspondence to: bryan_roth@med.unc.edu or rstracha@email.unc.edu.

#= Equal contribution

Author Contributions

R.H.J.O., J.F.D., J.G.E., B.L.R., and R.T.S. developed the concept and designed the experiments. R.H.J.O. and J.F.D. performed the bulk of the molecular biology and experimentation, with A.M.G., B.E.K., S.T.S., T.C., J.D.M., A.C.G., and R.T.S., contributing to the *in vitro* pharmacology assays. J.G.E. established the cloning strategy and helped with construct generation. R.H.J.O., J.F.D., J.G.E., B.L.R., and R.T.S. wrote and edited the manuscript. This work was supported by NIH grants R37DA035764, U24DK116195 and RO1MH112205 to B.L.R., and KO1MH109943 to R.T.S., and F31NS093917 to R.H.J.O., and the Michael Hooker Distinguished Professorship to B.L.R.

Competing Interests Statement

R.H.J.O., J.F.D., J.G.E., B.L.R., and R.T.S. are inventors of the TRUPATH technology, and could receive royalties. These relationships have been disclosed to and are under management by UNC-Chapel Hill.

Introduction

G Protein Coupled Receptors (GPCRs) represent not only the largest family of membrane targets for US Food and Drug Administration (FDA)-approved drugs[1] but are also among the most understudied drug targets in the human genome[1,2]. It is widely appreciated that GPCR ligands can bias receptor activity towards distinct intracellular G protein and arrestin pathways via a process known as functional selectivity or biased agonism[3,4]. Notably, biased agonists for κ-opioid[5] and μ-opioid[6], β-adrenergic[7], and other receptors[8] may provide therapeutic actions with fewer deleterious side-effects[9]. Accordingly, creating biased ligands that activate or attenuate specific G protein or arrestin signaling pathways represents a major area of research for chemical biologists, pharmacologists, and drug discovery scientists.

The complex signaling mechanisms that drive the therapeutic efficacy and side-effects of GPCR-targeted drugs remain largely unknown[10], thereby complicating efforts to create pathway-specific drugs. This is due, in part, to insufficiently robust and scalable assay platforms to interrogate multiple G proteins with single pathway resolution in cells. Such resolution is key as GPCRs can activate up to 16 different non-visual G protein transducers (collectively dubbed the transducerome) with considerable redundancy at the second messenger level. For instance, seven Gi/o class proteins are known to inhibit cAMP in cellular assays. A variety of bioluminescence resonance energy transfer (BRET)- and fluorescence resonance energy transfer (FRET)-based assays have been developed for different G protein family pathways[11,12] albeit they do not directly measure G protein activation. Although more direct BRET- and FRET-based assays for measuring activation of individual G protein subunits have been employed since 2001[13], no easily accessible and comprehensive set of Gαβγ FRET or BRET probes have been reported[14–19]. Additionally, of those that exist, relatively few have been fully optimized and characterized.

Here we report the results of a large-scale optimization and validation campaign aimed at developing robust BRET2-based biosensors to measure activation of non-visual G protein TRansdUcer PATHways, a platform that we have dubbed TRUPATH. Specifically, we optimized each component of the Gαβγ heterotrimer (i.e., 16 different Gα subunits, 4 major Gβ subunits, and 12 Gγ subunits) to develop a single readout biosensor platform covering 14 G protein pathways. In head-to-head studies, TRUPATH biosensors outperformed first-generation sensors at multiple GPCRs and in different cell lines. Benchmarking studies with TRUPATH biosensors recapitulated previously documented signaling bias and revealed new coupling preferences for prototypic and understudied GPCRs with potential *in vivo* relevance. To enable a greater understanding of GPCR molecular pharmacology by the scientific community, we have made TRUPATH biosensors easily accessible as a kit through Addgene (https://www.addgene.org/).

Results

Optimization of Gα-RLuc8/Gβ/Gγ-GFP2 biosensors

The proximal steps that initiate G protein signaling cascades include receptor-mediated guanine nucleotide exchange at the Gα-subunit of the Gαβγ heterotrimer and subsequent dissociation of the heterotrimeric complex. Heterotrimer dissociation ultimately leads to

effector activation and downstream cellular responses[20]. A decrease in the resonance energy transfer between fluorescently- (FRET) or luminescently (BRET or BRET2)-labeled heterotrimer subunits can detect dissociation and has been used as a proxy for direct measurements of ligand-receptor-transducer coupling[13,15,18] (Supplementary Figure 1A). Because optimal FRET and BRET probe pairs depend upon both the proximity of the donor and acceptor proteins and the orientation of their transition dipole moments (Supplementary Figure 1B), the *de novo* design of high-performing Gαβγ sensors is challenging and non-trivial. This is due in part to the diverse conformations and orientations of Gα and Gβγ subunits, especially in their inactive states[21]. Here we chose the variant BRET2 given its increased spectral resolution over BRET1 (~115nm vs 45–55nm, respectively). Although high-resolution structures can be used to identify potential regions for inserting donor or acceptor molecules based on proximity constraints, they cannot readily predict the conformational dynamics of the target proteins that might influence resonance energy transfer efficiency. Here we combined structure-guided protein engineering with exhaustive experimental refinement to afford optimal Gα-RLuc8 donor and Gβγ-GFP2 acceptor BRET2 pairs for 14 different human G proteins.

To limit the number of Gα-RLuc8 donor chimeras tested, we first targeted the flexible loop regions between the αA-αB and αB-αC helices in the α-helical domain of the Gα-subunit (Supplementary Figure 1C). While these regions are amenable to insertion of fluorescent[13,22] and luminescent[15] proteins, varying the insertion site can have unpredictable and sometimes deleterious effects on Gα protein function[23]. Accordingly, we generated between 12 and 20 RLuc8 insertions for each Gα subunit to sample every amino-acid position within these loops (Supplementary Figure 1D). To guide our approach, we relied on published crystal structures or homology models (Supplementary Table 1). Each Gα-RLuc8 chimeric donor was tested alongside standard Gβ1/Gγ2-GFP2 or Gβ1/Gγ1-GFP2 acceptor constructs and an appropriate model GPCR (e.g. NT_1R Neurotensin-1 receptor for Gαq-class G proteins) (Supplementary Figure 1E). The concentration-response curve for each chimera was then compared to the response of a reference Gα-RLuc8 chimera (i.e. RLuc8 inserted after the first lysine in the αA-αB linker domain; insertion of RLuc8 after Lys97 in Gαq was named Gαq(98)RLuc8). This reference site was chosen because of its use in many first-generation FRET, BRET, or BRET2 Gαβγ biosensors[13,15,23], which also represent the largest documented set to date. Of the top five performing Gα-RLuc8 chimeras, the Gα-RLuc8 that reproducibly exhibited the greatest dynamic range was then advanced to the Gβγ-GFP2 optimization phase (Supplementary Figure 1F).

Optimal Gβγ-GFP2 acceptors were subsequently identified through stepwise screening of 12 N-terminal Gγ-GFP2 fusions (Gγ1–13) and four wild-type Gβ subunits (Gβ1–4). Experimentally, Gγ screens included the optimal Gα-RLuc8 chimera, a co-precipitated mixture of wild-type Gβ1–4, a single Gγ-GFP2 test construct, and a model GPCR (Supplementary Figure 1G). The Gα-RLuc8/Gγ-GFP2 pair that exhibited the greatest dynamic range was then screened against each of four Gβ subunits (Supplementary Figure 1H). This stepwise optimization process was repeated for all G proteins to produce the final suite of TRUPATH Gα-RLuc8/Gβγ-GFP2 biosensors (Table 1, Supplementary Figure 1I, Supplementary Note).

The first fully optimized biosensor was Gαq. We defined the initial set of Gαq-RLuc8 insertions sites to be 98–105 and 116–126 within the loops connecting αA-αB and αB-αC helices, respectively (PDB 3AH8)[24](Figure 1A). For this initial screen we used γ1-GFP2 as the acceptor construct given its recent use with Gαq sensors[25] and NT_1R as the model receptor and truncated neurotensin (NT8–13) as the test agonist. RLuc8 insertion positions 119, 122, 123, 125, and 126 produced the greatest responses relative to the reference position 98 (squares, Figure 1B). RLuc8 insertion at 125 (Gαq(125)-RLuc8) was confirmed (Figure 1C) and advanced to the Gγ-GFP2 optimization phase. Screening Gαq(125)-RLuc8 against 12 Gγ-GFP2 chimeras identified Gγ1 and Gγ9 as the most optimal acceptor constructs (squares, Figure 1D). At the Gβ optimization phase, Gβ3 exhibited a slightly greater net BRET response in conjunction with Gγ9-GFP (squares, Figure 1E). As proof-of-concept, the resultant Gαq biosensor Gαq(125)-RLuc8/Gβ3γ9-GFP2 reported robust activation by a panel of canonically Gαq-coupled receptors (Supplementary Figure 2A). Finally, we confirmed that RLuc8 insertion did not compromise Gαq(125)-RLuc8 function in HEK293 cells lacking Gαq/11/12/13/s/Olf (HEK293ΔG) proteins[26]. As shown in Supplementary Figure 2B, NT_1R activated Gαq(125)-RLuc8 with a potency equal to the wild-type Gαq.

The same optimization workflow (Figure 1, Supplementary Figure 1F–I) was successfully applied to other human Gα-subunits (Supplementary Figures 3–11,13,15–17), including two first-in-class biosensors for Gα15 and GαGustducin. Optimization of Gαi1, Gαi2, Gαi3, GαZ, GαsShort, GαsLong, Gα12, and Gα13 identified new RLuc8 insertion sites that outperformed the reference positions; while the reference constructs for GαoA and GαoB were ultimately the most suitable sites (Table 1). Notably, apart from some of the closely related Gαi-class (Gαi1, Gαi2, GαoA and GαoB) and Gαs isoforms, we did not observe consistent patterns in optimal RLuc8 positioning. This demonstrates that a purely structure-guided or homology-based approach for generating Gα-RLuc8 chimeras is not likely to be successful and that optimal design is non-obvious. We also observed that the optimal Gβγ-GFP2 dimer constructs for most Gα-subunits was Gβ3γ9 and not the commonly used Gβ1γ2 or Gβ1γ1 dimers. Ultimately, we found that many combinations of Gβγ-GFP2 (e.g., Gβ3γ8, Gβ3γ1; Table 1) were superior to the acceptor combinations used in published biosensors, further confirming the validity of our empirical, unbiased approach.

We failed to detect substantial basal BRET2 responses or reproducible concentration-response curves for GαOlf, Gα11, Gα14, and Gα15 when inserting RLuc8 within the α-helical domain (Supplementary Figures 12–15). Using the crystal structure of the GDP-bound Gαq/Gβ1γ2 heterotrimer complex (3AH8), we identified alternative RLuc8 insertion sites, first focusing on Gα11 given its high identity (90%) and similarity (96%) to Gαq. After excluding residues and regions already interrogated, those with known secondary-structures, and those within flexible regions of Switch II because of its many sites of contact with the Gβ subunit, we identified a flexible loop region named Switch III that is situated between the β4-strand and the α3 helix of the Ras-like domain (Figure 2A). The closest Switch III residue to Gγ2 was a glutamic acid at position 241 (E241) (Figure 2A inset), a conserved amino-acid whose backbone carbonyl mediates interactions with RGS proteins[27] and that is involved in Gα signaling to downstream effectors but has no effect on receptor-mediated GTP-GDP exchange, GTP hydrolysis, nor physical binding to PDE[28]. Inserting

RLuc8 into this region (Gα11(241)-RLuc8) yielded a chimera that retained wild-type functionality in calcium mobilization assays in HEK293ΔG cells (Supplementary Figure 2C). We next generated and screened Gα11-RLuc8 constructs spanning the entire Switch III region (Figure 2B) using Gβ3/Gγ13-GFP2 as a suitable acceptor pair (Supplementary Figure 13E,F) (Figure 2C). We ultimately identified Gα11(246)-RLuc8/Gβ3γ13-GFP2 as the top-performing biosensor composition (Figure 2D–F). For completeness, we determined that the Gα11(246)-RLuc8 chimera recapitulated wild-type function in a calcium mobilization assay (Supplementary Figure 20E). Therefore, Switch III is a novel and fruitful region for Gα-protein engineering.

Targeting Switch III for the remaining G proteins yielded the first functional Gα15 biosensor (Supplementary Figure 15) but did not yield functional Gα14 (Supplementary Figure 14E) or GαOlf (Supplementary Figure 12F, position 244) biosensors. It was unlikely that exogenous Gα14 or GαOlf are non-functional as overexpression of these subunits activates effectors in HEK293T cells[25,29]. Based on the low basal BRET2 signals for both α-helical domain (Supplementary Figure 14B) and Switch III Gα14-RLuc8 chimeras (Supplementary Figure 14E), and the observation that replacing the entire α-helical domain of Gα14 with that of the Gαq(125)-RLuc8 construct did not produce a functional biosensor (Supplementary Figure 14F), we surmise that the engineered Gα14 heterotrimer is unstable or dysfunctional, or that Gα14 may exist predominantly dissociated from Gβγ. By contrast, GαOlf-RLuc8 chimeras exhibited good basal BRET2 (Supplementary Figure 12 A–C); however, these were not activated by canonically GαOlf-coupled receptors (e.g. Adenosine 2A, Gs-DREADD, Dopamine D1, or β_2AR receptors) (Supplementary Figure 12 A–C). Attempts to replicate recently published BRET2 biosensors for GαOlf[16] were similarly unsuccessful (Supplementary Figure 12D,E). Forced activation by treatment with cholera toxin produced an expected decrease in Gαs-mediated BRET2, but instead produced an increase in GαOlf BRET2 (Supplementary Figure 12F,G), despite a shared sensitivity and mechanism of action. The reasons for this remain unclear but likely reflect a stable, yet non-functional GαOlf heterotrimer.

Characterization of optimized G protein biosensors

To gauge their relative performance, we compared TRUPATH biosensors with published first-generation biosensors[15]. In the case of G proteins not part of this original set, equivalent RLuc8 chimeras were used. Using multiple model receptor systems, each TRUPATH biosensor outperformed its comparator with statistically significant improvements ranging from 1.5- to approximately 100-fold (Figure 3A–J, Supplementary Figure 18A,B,D,E Supplementary Table 2), with the median and mean improvement being 7.8- and 20.5-fold, respectively. As during the development process, GαOlf and Gα14 sensors failed to produce a concentration-response curve (Supplementary Figure 18C,F). To compensate for any receptor-dependent effects, we also performed a head-to-head comparison using the AT_1R Angiotensin II receptor as previously reported[15]. As shown in Supplementary Figure 19, TRUPATH biosensors statistically outperformed first-generation sensors at most pathways. Significantly, AngII-mediated activation of Gα11 and Gα12 was completely missed by first-generation biosensors but yielded robust responses at corresponding TRUPATH sensors (Supplementary Figure 19H,I), suggesting that AT_1R is not biased against Gα12 as

previously determined[15]. Together, these comparisons demonstrate the enhanced performance and importance of using optimized G protein biosensors.

We next determined if TRUPATH biosensors could detect inverse agonism given that baseline BRET2 response reflects the equilibrium of associated/dissociated Gαβγ heterotrimer. For these experiments we chose the Gi-coupled cannabinoid-1 receptor (CB_1R) that exhibits high constitutive activity[30]. As shown in Supplementary Figure 20A for our optimized Gαi3 biosensor, the inverse-agonist rimonabant caused a very large decrease in normalized CB_1R constitutive activity, while the full agonist WIN 55,212–2 produced a comparably weaker increase in activity (Supplementary Table 3). These data support the sensitive detection of inverse agonism using TRUPATH biosensors.

Ligand parameters of potency (EC_{50}) and efficacy (E_{max}) are greatly modulated by the level of receptor reserve and by amplification of the stimulus-response cascade, both of which complicate efforts to accurately characterize ligand pharmacology and quantify ligand bias[31]. Because heterotrimeric BRET2 sensors measure pathway activation proximal to the receptor, we posited that amplification should be minimal, although receptor reserve could be operative. To test this, we eliminated spare receptors via receptor-alkylation. We found that depletion of the μ-opioid receptor (μOR) with increasing concentrations (0–30 nM) of the irreversible antagonist β-funaltrexamine[32] (β-FNA) significantly reduced the maximal response (E_{max}) of the full agonist DAMGO, with a modest effect on potency (Supplementary Figure 20B–D, Supplementary Table 3). Specifically, we identified a trend of decreasing EC_{50} values with increasing β-FNA concentration ($F(1,52) = 6.793$, $p = 0.0119$), but with a small effect size ($r^2 = 0.1005$), suggesting that the observed effect is likely real but small. Conversely, the effect of increasing concentrations of β-FNA on the maximum response was large and immediate ($F(1,52) = 180.6$, $p < 0.0001$; $r^2 = 0.7502$). Taken together, these data suggest that TRUPATH assays exhibit minimal amplification and/or receptor reserve under the conditions used here. In direct support of this, radioligand binding assays confirmed receptor density to be quite modest (219 +/− 5 fmol/mg; mean +/− SEM, n=3). Thus, TRUPATH biosensors provide accurate measurements of ligand potency and efficacy without the need for post-processing methods[33], which is ideal for quantifying functional selectivity across the human transducerome.

We also controlled for the possibility that Gα-RLuc8 chimeras were functionally compromised by comparing a subset of Gα-RLuc8 sensors covering three major effector classes to their wild-type counterparts in standard second-messenger assays. The Gαq, Gα11, Gα15, Gαi3, GαZ, and Gαs TRUPATH sensors performed similarly to, and were statistically indistinguishable from, their wild-type counterparts (Supplementary Figure 2B, Supplementary Figure 20E–H, Supplementary Table 3), demonstrating that our biosensors recapitulate wild-type functionality.

Interrogating the human G-protein transducerome

TRUPATH biosensors were developed to comprehensively profile GPCR coupling preferences. Here we profiled a panel of well-studied and understudied GPCRs and their endogenous ligands in HEK293T (Figure 4) and CHO cells (Supplementary Figure 22). To account for variation between experiments, the NT_1R neurotensin receptor served as a

reference standard for all G proteins except GαGustducin and Gαs isoforms, for which the κOR and the β_2-adrenergic receptor (β_2AR) were used, respectively.

We first profiled the prototypic β_2AR and its endogenous agonist epinephrine in HEK293T cells. In addition to the expected coupling to canonical Gαs-family proteins, modest coupling to Gαi-class transducers was detected, as previously reported (Figure 4, Supplementary Figure 21A). We observed remarkable restriction of epinephrine activity to a subset of Gαi-class proteins including Gαi2, GαoA, GαoB, and GαZ, suggesting that the receptor-transducer interface differentiates between functionally similar G proteins. We confirmed that activation of the Gαi2 TRUPATH sensor was due to exogenous β_2AR and not endogenous adrenergic receptors by substituting pcDNA for β_2AR and treating with epinephrine or the α_2-adrenergic receptor-selective agonist clonidine (Supplementary Figure 21B). Similarly, the β_2AR-selective agonist isoproterenol activated Gαi2 (Supplementary Figure 21B). In confirmation of earlier reports[34], the epinephrine-activated β_2AR also coupled to Gα15 with moderate efficacy (Figure 4B) and greater potency (Figure 4A) compared to other G protein pathways (Supplementary Figure 21A, Supplementary Datasets 1–3). Accordingly, epinephrine elicited calcium responses in HEKΔG cells that was blocked by the βAR antagonist alprenolol (Supplementary Figure 21C).

We next profiled the well-studied (NT_1R) and less thoroughly interrogated (LPA_6 lysophosphatidic acid and 5-HT_7 serotonin) receptors using their respective endogenous agonists neurotensin (8–13), 1-oleoyl lysophosphatidic acid (LPA), and serotonin (5-HT). The NT_1R coupled to nearly all G-proteins except for the Gαs isoforms (Figure 4B). By contrast, LPA_6R coupling was restricted to subsets of Gαi isoforms, Gα12/13, and minimally to GαsShort. While the discrepancy between GαsShort and GαsLong coupling was notable as they are isoforms, the low solubility of LPA precluded testing at higher concentrations that might have otherwise revealed weak coupling to GαsLong. The 5-HT_7 receptor exhibited the greatest selectivity of the four receptors, coupling exclusively to both Gαs isoforms (Figure 4B).

We controlled for cell-type differences in TRUPATH biosensor performance by profiling endogenous agonists at the β_2AR and NT_1R in CHO cells. As shown in Supplementary Figure 22 (values reported in Supplementary Table 5), we reproduced primary coupling of the β_2AR to GαsShort, GαsLong, and Gα15; whereas weaker secondary coupling to Gi/o class proteins was not observed, which we attributed to lower expression of BRET2 biosensor components as we observed consistently reduced luminescent signal in these experiments. By contrast, we reproduced the extreme promiscuity of NT_1R in CHO cells originally seen in HEK293T cells (Figure 4). Altogether, the increased transfection efficiency or greater expression of biosensor components in HEK293T cells appears to confer greater sensitivity to detect weaker coupling events and remains the preferred cell system for TRUPATH profiling.

Large-scale transducerome drug screening

TRUPATH biosensors are ideally suited for screening chemically diverse compounds at a single receptor across the human G protein transducerome. The κOR was selected because

of renewed interest in identifying κOR-targeted therapies[5] and its diverse physiological effects including analgesia, anxiety, itch, and hallucinations.

Traditional methods for quantifying ligand-receptor-transducer bias[35] account for differences between two pathways (e.g. arrestin vs G protein) but are not readily scaled to interpret multidimensional data of this type. Specifically, transduction coefficients ($log\left(\frac{EMax}{EC50}\right)$) are inappropriate for scenarios involving partial agonists and when the reference agonist is not maximally efficacious across all pathways tested[35], which is particularly relevant as TRUPATH assays experience minimal signal amplification and are comprehensive. Transduction coefficients also mask the individual contributions of E_{max} and EC_{50} to bias, which are important considerations when developing affinity- or efficacy-biased ligands[10] and for building detailed structure-activity-relationships. Here we consider potency and efficacy (reported in Supplementary Table 4) as separate contributing factors to a ligand's overall manifestation of signaling bias.

The κOR transducer coupling profile for this ligand set was entirely restricted to the Gαi/o effector class, within which we detected a statistically significant range of potency (Figure 5A) and efficacy (Figure 5B) values (Supplementary Table 4 and Supplementary Datasets 4–6). This supports our assertion that distinctions in signaling preferences or functional selectivity exist for even the most well-studied receptor systems when screening the transducerome. Specifically, a recurring pattern for many κOR ligands was greater potency at GαZ and weaker potency at GαGustducin (Figure 5A), which we do not attribute to artifacts of a particular biosensor as this pattern did not extend to all the ligands and receptors examined here. For example, at the β_2AR receptor epinephrine exhibited significantly greater potency (120-fold) for the Gα15 pathway relative to Gαi2, a difference that was not observed between these same transducers at NT_1R (Figure 4A, Supplementary Datasets 1,3). Additionally, during the optimization and validation stages of the project we observed enhanced potency of the μOR agonist DAMGO at GαZ relative to Gαi3, which was consistent in both BRET2 (Supplementary Figure 5D and 8D) ($t(4) = 10.11$, $p = 0.0005$) and Glosensor cAMP assays ($t(4) = 14.20$, $p = 0.0001$) (Supplementary Figure 20G, Supplementary Table 3).

Salvinorin A, U69,593, GR89696, ML139, and RB64 exhibited uniform efficacies across transducers (Figure 5B, Supplementary Figure 23, Supplementary Dataset 4); whereas other ligands exhibited a range of partial agonism between G protein pathways (Figure 5B, Supplementary Dataset 4) that varied from small (BU74, Figure 5B, Supplementary Figure 23D) to more extreme differences (Diprenorphin, Figure 5B, Supplementary Figure 23G). Remarkably, the endogenous agonist Dynorphin A (1–13)—a relatively efficacious partial agonist at most transducers—was nearly inactive at GαGustducin (Figure 5B, Supplementary Figure 23E). Notably, the strongly G protein-biased κOR ligand RB64[5,36] exhibited the least variation in both potency and efficacy across the transducerome (Figure 5B, Supplementary Figure 23H).

We endeavored to expand the pharmacologist's toolkit and make readily available an assay platform that enables deep biological insight. While our assay identifies sets of possible coupling events, the question of biological relevance remains: how likely is *in vitro* coupling

to translate *in vivo*? In a proof-of-concept experiment, we tested the *in vivo* relevance of our unanticipated finding that the κOR robustly activates the taste receptor transducer GαGustducin (Figure 5). It was previously reported that activation of a chemogenetic κOR mutant (Ro1) in TAS2R-expressing cells of the tongue mediated bitter taste perception[37]. It was inferred that Ro1, like endogenous TAS2Rs, signaled through GαGustducin to produce this response. Using our GαGustducin biosensor, we confirmed that both the WT κOR and the chemogenetic κOR Ro1 activated canonical Gαi3 and novel GαGustducin transducers to a similar extent (Supplementary Figure panels 24A and 24B, respectively). These data provide the first mechanistic support for the aversive behavioral response observed by Mueller et al., 2005[37] and suggest that *in vitro* profiles can translate to the *in vivo* setting.

Discussion

Here we present the TRUPATH suite of 14 optimized BRET2 biosensors (Table 1 and Supplementary Note) that affords near complete coverage of the human G protein transducerome with enhanced dynamic range compared to first-generation sensors[15]. While some first-generation BRET2 Gα-RLuc8 chimeras performed reasonably well in our hands (e.g., GαoA, GαoB; Figure 3 and Supplementary Figures 6,7, and 18), others failed to report reliable or substantial dynamic ranges (e.g. Gs, G11, G12 and G13; Figure 3, Supplementary Figures 10,11,13,16,17). Even related transducers, such as the highly homologous Gαq and Gα11 proteins, showed distinctions regarding their performance and amenability to protein engineering (Figures 2,3, Supplementary Figure 13). It is thus likely that even small differences in amino-acid composition have unpredictable effects on structure or conformational dynamics that are not predicted from their primary sequences or structures. These issues, together with a general pattern of suboptimal performance of many published constructs[16,18], support the rigorous empirical process deployed here to develop TRUPATH biosensors. More broadly, the non-obvious nature of optimal donor-acceptor positioning likely means that a similarly exhaustive approach would benefit the engineering of other RET systems.

While much has been done to elucidate the molecular and structural basis for arrestinergic vs. G protein signal transduction[38], as well as the physiological significance of these divergent pathways[6], relatively little is known about the consequences of “non-canonical” G protein signaling. Thus, similar to the ‘dark’ regions of the genome[2], the transducerome profiles of most GPCRs remain unexplored, which likely conceals fundamental biology and new therapeutic approaches. It is a matter of observation that similar Gα isoforms exhibit diverse expression patterns ranging from largely ubiquitous[39] to tissue-restricted[40]. The selective signal transduction profiles of different ligands provide additional layers of complexity to tissue-specific signal transduction and, potentially, afford new opportunities for drug discovery. Although the biological relevance of these Gα-biased signaling events remains to be established in target tissues and organs, what is clear from this study and others[41] is that GPCRs are more promiscuous in their coupling preferences than previously imagined. Whether this “switching” of Gα-coupling for GPCRs arises as a consequence of modifications such as phosphorylation[42] or is an intrinsic property of a receptor-ligand system, it is evident that much can be learned from a detailed exploration of the transducerome.

The recent work of Sandhu et al.[43] used molecular dynamics (MD) simulations and Gα C-terminal peptides to show that GPCRs possess latent intracellular G protein binding cavities with varying propensities to bind cognate and non-cognate G proteins. Within this framework, promiscuously coupled receptors like the NT_1R neurotensin receptor tested here are likely to have latent binding cavities with energetically favorable hotspots that attract many G protein C-termini to yield tight and productive coupling. Conversely, highly selective GPCRs like the 5-HT_7 serotonin receptor likely have latent cavities optimized for strong interactions with one or a few G proteins. A contemporaneous study by Okashah et al.[44] looked at the coupling of 12 C-terminal Gα chimeras and 4 full-length G proteins, from which they derived universal guidelines for G protein coupling, e.g. Gαi-coupled receptors are less promiscuous than Gαs- and Gαq-coupled receptors, amongst others. However, from the small number of transducerome profiles generated here (Figure 4), we could not corroborate these general guidelines. Specifically, we failed to observe universal Gαi1 coupling (e.g. 5-HT_7), Gαq coupling for Gs-coupled receptors (e.g. 5-HT_7, and β_2AR), and restricted coupling preferences for all Gαi1-coupled receptors (e.g. NT_1R). These differences likely reflect our use of full-length G proteins and a readout that requires G protein activation (i.e. dissociation or rearrangement of the heterotrimeric sensor). By contrast, both of the above studies relied mainly on Gα C-termini to drive coupling, which does not account for the influence of the Gα subunit core[44]. Moreover, the formation of stable complexes between agonist-occupied receptors and nucleotide-free G proteins is likely detecting weak secondary coupling too inefficient to register as activation in our assay[44].

The optimized heterotrimer compositions for each Gα protein might shed light on endogenous Gβ and Gγ subunit preferences. Indeed, reports have suggested preferred combinations of Gα subunits and specific Gβγ dimers (e.g. between GαOlf and Gβ2 and Gγ7[45]). However, a surprisingly limited number of non-canonical Gβγ combinations were the preferred acceptors for most Gα-RLuc8 donors (Table 1). Given that TRUPATH sensor compositions were selected for maximal RET efficiency, it is likely that these biosensor compositions do not represent preferred endogenous heterotrimers, but instead reflect optimal subunit positioning and/or complex stability for maximal RET. This predicts that targeting different regions of the Gα for RLuc8 insertion would yield region-specific Gβγ dimer preferences. Indeed, Gβ3 and Gγ8-GFP2 or Gγ9-GFP2 were the preferred partners for nearly all BRET2 biosensors when RLuc8 was inserted within the Gα α-helical domain. By contrast, RLuc8 insertion within the newly targeted Switch III region of Gα11 and Gα15 selected exclusively for the Gβ3Gγ13-GFP2 dimer. Related to this, it is possible that the different TRUPATH Gαβγ combinations chosen during optimization influence receptor coupling preferences. We find this unlikely, however, considering our ability to reproduce the canonical coupling preferences and previously reported bias for the GPCRs tested here. Furthermore, we identified non-canonical coupling of the β_2AR to Gα15 via the TRUPATH Gα15 biosensor (Gα15(245)-RLuc8/Gβ3γ13-GFP2) and then verified this coupling via cell-based Ca^{2+} assays in the absence of exogenous Gβ3Gγ13 (Supplementary Figure 21C). We have made available through Addgene all four Gβ and all 12 Gγ-GFP constructs to accommodate the use of other heterotrimer combinations.

It is worth mentioning that, not unlike other cell-based platforms, TRUPATH biosensors identify the potential for biased agonism for any given ligand-GPCR pair. How this bias translates to a physiological response in the target cell or tissue (i.e. how the cell interprets this 'stimulus') is uncertain as it depends on expression of the requisite signal transduction machinery. Thus, combining TRUPATH profiling with multi-omics strategies could enhance our ability to predict the *in vivo* consequences of *in vitro* bias profiles.

In conclusion, the open-source TRUPATH platform represents the most robust, complete, and thoroughly documented suite of Gαβγ-based GPCR signaling biosensors available to date. Each biosensor represents either a novel assay for a previously untargeted G protein pathway (Gα15 and GαGustducin) or, to our knowledge, the most optimized heterotrimer-based BRET2 sensor for previously documented pathways[14,15]. We documented each step of the development and optimization process to encourage adoption of these tools as a common component in the GPCR screening toolkit. Screening tools such as these that provide single pathway resolution will empower consistent and reliable measurements reflective of true signaling preferences. Such insights will undoubtedly accelerate efforts to illuminate the druggable GPCRome[8,46,47] and to understand the consequences of biased G protein signaling.

Online Methods

Cloning and Molecular Biology

Plasmids containing human Gα constructs were obtained from the cDNA Resource Center (www.cDNA.org), except for Gα12 and GαGustducin, which were synthesized as gene blocks by Integrated DNA Technologies, IDT (Coralville, IA). Plasmids containing the κOR RASSL Ro1, Gβ2–4 and Gγ1,3–13 were obtained from Addgene (Watertown, MA), except for Gβ1 and Gγ2-GFP2 which were a gift from Dr. Michel Bouvier at Université de Montréal, Montréal, Quebec, Canada. Gα constructs were subcloned into pCDNA5/FRT/TO, while Gβ and Gγ constructs were subcloned into pcDNA 3.1. Receptor constructs were generated by deleting the vasopressin 2 receptor C-terminus and tTa sequence from receptor plasmids from the PRESTO-TANGO library[1].

Chimeric constructs (e.g. Gα-RLuc8 and Gγ-GFP2 constructs) were generated via HiFi DNA assembly (New England Biolabs, Ipswich, MA). Gγ-GFP2 constructs were generated by amplification of the backbone construct (e.g. pcDNA-Gγ) from the N-terminal start codon and adding homology to the C-terminus of GFP2 flanked by a short flexible linker sequence (GSAGT). GFP2 sequences were amplified by PCR, adding homology to the pcDNA backbone at the 5' end, and homology to the N-terminus of the Gγ sequence at the 3' end. Backbone and insert constructs were co-incubated with HiFi master mix and transformed into Stbl3 *E. coli* (ThermoFisher Scientific, Waltham, MA). Gα-RLuc8 chimeras were generated by linearizing a single backbone template for each region (e.g. αA-αB linker region, αB-αC helical region, switch III), amplifying outwards from the 5' and 3' ends of the beginning of those respective regions—producing a linearized construct lacking that sequence. These deleted codons were filled in with RLuc8 insertion sequences by overhang PCR while adding a flexible SGGGS linker, the missing codon sequences flanking the appropriate insertion site, and homology to the 5' and 3' end of the linearized backbone.

These were incubated with HiFi master mix to assemble Gα-RLuc8 chimeras containing a fully intact Gα with an RLuc8 sequence, one for each amino-acid position within the targeted region. The sequence of each Gα-RLuc8 chimera can be found in the Supplemental Note.

Pertussis insensitive Gαi3 (C351I) was generated by PCR mutagenesis.

Cell culture

HEK293T cells were obtained from ATCC (Manassas, VA). HEK293ΔGQ/11/12/13/s/Olf cells were a generous gift from Dr. Asuka Inoue at Tohoku University, Sendai, Japan. Cells were maintained, passaged, and transfected in DMEM medium containing 10% FBS, 100 Units/mL penicillin, and 100μg/mL streptomycin (Gibco-ThermoFisher, Waltham, MA) in a humidified atmosphere at 37°C and 5% CO2. After transfection, cells were plated in DMEM containing 1% dialyzed FBS, 100 Units/mL penicillin, and 100μg/mL streptomycin for BRET2, calcium, and GloSensor assays.

BRET2 assays

Cells were plated either in six-well dishes at a density of 700,000–800,000 cells/well, or 10-cm dishes at 7–8 million cells/dish. Cells were transfected 2–4 hours later, using a 1:1:1:1 DNA ratio of receptor:Gα-RLuc8:Gβ:Gγ-GFP2 (100 ng/construct for six-well dishes, 750 ng/construct for 10-cm dishes), except for the Gγ-GFP2 screen, where an ethanol co-precipitated mixture of Gβ1–4-was used at twice its normal ratio (1:1:2:1). Transit 2020 (Mirus Biosciences, Madison, WI) was used to complex the DNA at a ratio of 3 μL Transit/μg DNA, in OptiMEM (Gibco-ThermoFisher, Waltham, MA) at a concentration of 10 ng DNA/μL OptiMEM. The next day, cells were harvested from the plate using Versene (0.1M PBS + 0.5 mM EDTA, pH 7.4), and plated in poly-D-lysine-coated white, clear bottom 96-well assay plates (Greiner Bio-One, Monroe, NC) at a density of 30,000–50,000 cells/well.

One day after plating in 96-well assay plates, white backings (Perkin Elmer, Waltham, MA) were applied to the plate bottoms, and growth medium was carefully aspirated and replaced immediately with 60 μL of assay buffer (1x HBSS + 20 mM HEPES, pH 7.4), followed by a 10 μL addition of freshly prepared 50 μM coelenterazine 400a (Nanolight Technologies, Pinetop, AZ). After a five-minute equilibration period, cells were treated with 30 μL of drug for an additional 5 minutes. Plates were then read in an LB940 Mithras plate reader (Berthold Technologies, Oak Ridge, TN) with 395 nm (RLuc8-coelenterazine 400a) and 510 nm (GFP2) emission filters, at 1 second/well integration times. Plates were read serially six times, and measurements from the sixth read were used in all analyses. BRET2 ratios were computed as the ratio of the GFP2 emission to RLuc8 emission.

Calcium Mobilization Assays

Cells were plated in 10-cm plates as described in the BRET2 protocol and co-transfected with receptor (1 μg) and Gα-subunit (1μg) cDNA. The next day, cells were plated at 15,000 cells/well in poly-D-lysine coated black, clear bottom 384-well plates (Greiner Bio-One, Monroe, NC). The following day, growth medium was aspirated and replaced with 20 μL assay buffer containing 1x Fluo-4 Direct Calcium Dye (ThermoFisher Scientific, Waltham,

MA) and incubated for 60 minutes at 37°C (no CO_2). Plates were brought to RT for 10 minutes in the dark before being loaded into a FLIPR Tetra® liquid-handling robot and plate reader (Molecular Devices, San Jose, CA). Baseline fluorescence measurements were taken for 10 seconds followed by robotic drug addition (10 μL) and a 60-second measurement (1 measurement/second). For antagonist assays, cells were first treated with antagonist and kept in the dark at room temperature for ten minutes before agonist addition by the FLIPR Tetra® robot. Maximal response during this time was used to calculate amplitude of the calcium transients. Measurements were analyzed as percentage of maximum signal amplitude for the construct.

Glosensor cAMP Assays

Cells were plated in 10-cm plates as previously described. Cells were transfected with plasmids encoding cDNA for the Glosensor reporter (Promega, Madison, WI), receptor, and Gα-subunit at a ratio of 2:1:1 (2 μg: 1 μg: 1μg). The next day, cells were plated in black, clear-bottom, 384-well white plates. After aspiration of the medium on the day of the assay, cells were incubated for 60 minutes at 37°C with 20 μL of 5 mM luciferin substrate (GoldBio, St. Louis, MO) freshly prepared in assay buffer. For Gαs activity, 10 μL of drugs were added using the FLIPR Tetra® liquid-handling robot and read after 15 minutes in a Spectramax luminescence plate reader (Molecular Devices, San Jose, CA) with a 0.5 second signal integration time. For Gαi activity, 10 μL of drugs were added for a 15-minute incubation period. Subsequently, 10 μL of isoproterenol (final concentration of 200 nM) was added and incubated for an additional 15-minute period before reading.

Receptor Density Measurements

HEK293T cells were plated in 10cm dishes and transfected with the μOR and Gαi3 biosensor plasmids according to the BRET2 method detailed above. At 48 hr after transfection, membranes for radioligand binding were freshly prepared via hypotonic lysis. Specifically, cells were washed once with 10mL cold PBS and scraped into 10mL cold PBS. Cells were collected at 220 × g for 15min at 4°C and the supernatant was discarded. The cell pellet was resuspended in 600μL of cold hypotonic lysis buffer (50mM TrisHCl, pH 7.4), triturated, and aliquoted (100μL) into 1.5mL tubes. The crude membranes were collected at 15,000 × g for 30min at 4°C. The supernatant was discarded, and the membrane pellets were stored at −80°C.

Receptor density (fmol/mg protein) was measured via homologous competition binding assays in Prism (Graphpad Software, San Diego, CA). Competition assays were performed in round-bottom 96-well plates (Greiner) using standard binding buffer (50mM TrisHCl, 10mM $MgCl_2$, 0.1mM EDTA, 0.1% fatty acid-free BSA, 1mM ascorbic acid, pH7.4) containing two concentrations (~0.8nM and 3nM) of [^{3}H]Naloxone (70Ci/mmol, PerkinElmer), serial dilutions of cold naloxone competitor (10μM to 0.001nM), and 19.5mg of μOR + Gαi3 membrane. Pseudo-first order assumptions were met by using membranes at concentrations that bound <10% of the radioligand added to each well as determined from pilot assays. Non-specific binding was determined in the presence of 10μM naloxone. Plates were incubated at RT in the dark for 1.5hr and a PerkinElmer Filtermate harvester (PerkinElmer) was used to collect membranes onto 0.3% polyethyleneimine-treated GF/B

glass fiber filtermats that were washed 4X with cold buffer (50mM TrisHCl, pH7.4 at 4°C). The filters were dried, permeated with Meltilex scintillant (PerkinElmer), and counted on a Microbeta plate reader at 1min/well. Competition curves using different tracer concentrations were simultaneously fit to the homologous competition equation in Prism (GraphPad) to yield equilibrium dissociation constants (K_D) and Bmax (fmol/mg).

Data Analysis

All concentration-response curves were fit to a three-parameter logistic equation in Prism (Graphpad Software, San Diego, CA). BRET2 concentration-response curves were analyzed as either raw net BRET2 (fit Emax-fit Baseline) or by normalizing to a reference agonist for each experiment. Efficacy (Emax) calculations were performed according to Kenakin 2012[35]: stimulus-response amplitudes (net BRET2) were normalized to the maximal responding agonist (maximal system response). EC50 and Emax values were estimated from the simultaneous fitting of all biological replicates. Transduction coefficients were calculated as $Log\frac{EMax}{EC50}$ as described in Kenakin 2012[35] and propagation of error was conducted at all steps[48]. EC50, Emax, and transduction coefficient values were analyzed first by ANOVAs (F-test of curve fit, one-way ANOVA, or two-way ANOVA as described in the text). *Post hoc* pair-wise comparisons used Tukey-adjusted *p* values to control for multiple comparisons. Significance threshold was set at $\alpha = 0.05$.

Data Availability Statement

All data that were generated or analyzed during this study are included in this published article (and its Supplementary Information files) or are available from the corresponding authors upon reasonable request. All TRUPATH sensors are available to academic and non-profit institutions as a kit through Addgene (https://www.addgene.org/).

Supplementary Material

Refer to Web version on PubMed Central for supplementary material.

Acknowledgements

We would like to thank Dr. Michel Bouvier for the generous gift of the Gβ1 and Gγ2-GFP2 constructs. We would also like to thank Dr. Terry Kenakin for his insight on quantitative pharmacology. We would also like to thank Dr. Jeff Aubé for the generous gift of ML139. We would also like to thank Dr. Asuka Inoue for the generous donation of the HEK293ΔG cells. Due to space constraints we could not include all citations, for this we apologize.

References

1. Kroeze WK et al. PRESTO-TANGO: an open-source resource for interrogation of the druggable human GPCR-ome. Nat Struct Mol Biol 22, 362–369 (2015). [PubMed: 25895059]
2. Rodgers G et al. Glimmers in illuminating the druggable genome. Nat Rev Drug Discov 17, 301–302 (2018). [PubMed: 29348682]
3. Roth BL & Chuang D-M Multiple mechanisms of serotonergic signal transduction. Life Sciences 41, 1051–1064 (1987). [PubMed: 2441225]
4. Urban JD et al. Functional selectivity and classical concepts of quantitative pharmacology. J. Pharmacol. Exp. Ther 320, 1–13 (2007). [PubMed: 16803859]

5. White KL et al. The G Protein–Biased κ-Opioid Receptor Agonist RB-64 Is Analgesic with a Unique Spectrum of Activities In Vivo. J Pharmacol Exp Ther 352, 98–109 (2015). [PubMed: 25320048]
6. Manglik A et al. Structure-based discovery of opioid analgesics with reduced side effects. Nature 537, 185–190 (2016). [PubMed: 27533032]
7. Wisler JW et al. A unique mechanism of beta-blocker action: carvedilol stimulates beta-arrestin signaling. Proc Natl Acad Sci U S A 104, 16657–16662 (2007). [PubMed: 17925438]
8. Wacker D, Stevens RC & Roth BL How Ligands Illuminate GPCR Molecular Pharmacology. Cell 170, 414–427 (2017). [PubMed: 28753422]
9. Viscusi ER et al. A randomized, phase 2 study investigating TRV130, a biased ligand of the μ-opioid receptor, for the intravenous treatment of acute pain. Pain 157, 264–272 (2016). [PubMed: 26683109]
10. Kenakin T Biased Receptor Signaling in Drug Discovery. Pharmacol Rev 71, 267–315 (2019). [PubMed: 30914442]
11. Masuho I, Martemyanov KA & Lambert NA Monitoring G Protein Activation in Cells with BRET in *G* Protein-Coupled Receptors in Drug Discovery: Methods and Protocols (ed. Filizola M) vol. 1335 107–113 (Springer New York, 2015).
12. Wan Q et al. Mini G protein probes for active G protein–coupled receptors (GPCRs) in live cells. J. Biol. Chem 293, 7466–7473 (2018). [PubMed: 29523687]
13. Janetopoulos C, Jin T & Devreotes P Receptor-mediated activation of heterotrimeric G-proteins in living cells. Science 291, 2408–2411 (2001). [PubMed: 11264536]
14. Busnelli M et al. Functional selective oxytocin-derived agonists discriminate between individual G protein family subtypes. J. Biol. Chem 287, 3617–3629 (2012). [PubMed: 22069312]
15. Saulière A et al. Deciphering biased-agonism complexity reveals a new active AT1 receptor entity. Nat. Chem. Biol 8, 622–630 (2012). [PubMed: 22634635]
16. Yano H et al. Development of novel biosensors to study receptor-mediated activation of the G-protein α subunits Gs and Golf. J. Biol. Chem 292, 19989–19998 (2017). [PubMed: 29042444]
17. Adjobo-Hermans MJ et al. Real-time visualization of heterotrimeric G protein Gq activation in living cells. BMC Biol 9, 32 (2011). [PubMed: 21619590]
18. Mastop M et al. A FRET-based biosensor for measuring Gα13 activation in single cells. PLoS One 13, e0193705 (2018). [PubMed: 29505611]
19. van Unen J et al. A New Generation of FRET Sensors for Robust Measurement of Gαi1, Gαi2 and Gαi3 Activation Kinetics in Single Cells. PLoS One 11, (2016).
20. Gether U & Kobilka BK G protein-coupled receptors. II. Mechanism of agonist activation. J. Biol. Chem 273, 17979–17982 (1998). [PubMed: 9660746]
21. Smrcka AV et al. NMR analysis of G-protein βγ subunit complexes reveals a dynamic Gα-Gβγ subunit interface and multiple protein recognition modes. Proc Natl Acad Sci U S A 107, 639–644 (2010). [PubMed: 20018744]
22. Hughes TE, Zhang H, Logothetis DE & Berlot CH Visualization of a functional Galpha q-green fluorescent protein fusion in living cells. Association with the plasma membrane is disrupted by mutational activation and by elimination of palmitoylation sites, but not be activation mediated by receptors or AlF4-. J. Biol. Chem 276, 4227–4235 (2001). [PubMed: 11076942]
23. Gibson SK & Gilman AG Giα and Gβ subunits both define selectivity of G protein activation by α2-adrenergic receptors. Proc Natl Acad Sci U S A 103, 212–217 (2006). [PubMed: 16371464]
24. Nishimura A et al. Structural basis for the specific inhibition of heterotrimeric Gq protein by a small molecule. PNAS 107, 13666–13671 (2010). [PubMed: 20639466]
25. Schrage R et al. The experimental power of FR900359 to study Gq-regulated biological processes. Nat Commun 6, 10156 (2015). [PubMed: 26658454]
26. Grundmann M et al. Lack of beta-arrestin signaling in the absence of active G proteins. Nat Commun 9, 341 (2018). [PubMed: 29362459]
27. Tesmer JJ, Berman DM, Gilman AG & Sprang SR Structure of RGS4 bound to AlF4--activated G(i alpha1): stabilization of the transition state for GTP hydrolysis. Cell 89, 251–261 (1997). [PubMed: 9108480]

28. Li Q & Cerione RA Communication between Switch II and Switch III of the Transducin α Subunit Is Essential for Target Activation. J. Biol. Chem 272, 21673–21676 (1997). [PubMed: 9268292]
29. Kwan DHT, Yung LY, Ye RD & Wong YH Activation of Ras-dependent signaling pathways by G(14) -coupled receptors requires the adaptor protein TPR1. J. Cell. Biochem 113, 3486–3497 (2012). [PubMed: 22711498]
30. Felder CC et al. Comparison of the pharmacology and signal transduction of the human cannabinoid CB1 and CB2 receptors. Mol. Pharmacol 48, 443–450 (1995). [PubMed: 7565624]
31. Kenakin T Gaddum Memorial Lecture 2014: receptors as an evolving concept: from switches to biased microprocessors. Br J Pharmacol 172, 4238–4253 (2015). [PubMed: 26075971]
32. Rothman RB et al. beta-FNA binds irreversibly to the opiate receptor complex: in vivo and in vitro evidence. J. Pharmacol. Exp. Ther 247, 405–416 (1988). [PubMed: 2846819]
33. Kenakin T Functional Selectivity and Biased Receptor Signaling. J Pharmacol Exp Ther 336, 296–302 (2011). [PubMed: 21030484]
34. Innamorati G et al. Heterotrimeric G proteins demonstrate differential sensitivity to β-arrestin dependent desensitization. Cellular Signalling 21, 1135–1142 (2009). [PubMed: 19275934]
35. Kenakin T, Watson C, Muniz-Medina V, Christopoulos A & Novick S A Simple Method for Quantifying Functional Selectivity and Agonist Bias. ACS Chem Neurosci 3, 193–203 (2011). [PubMed: 22860188]
36. White KL et al. Identification of novel functionally selective κ-opioid receptor scaffolds. Mol. Pharmacol 85, 83–90 (2014). [PubMed: 24113749]
37. Mueller KL et al. The receptors and coding logic for bitter taste. Nature 434, 225–229 (2005). [PubMed: 15759003]
38. Wacker D et al. Crystal Structure of an LSD-Bound Human Serotonin Receptor. Cell 168, 377–389.e12 (2017). [PubMed: 28129538]
39. Garibay JLR et al. Analysis by mRNA levels of the expression of six G protein α-subunit genes in mammalian cells and tissues. Biochimica et Biophysica Acta (BBA) - Molecular Cell Research 1094, 193–199 (1991). [PubMed: 1654117]
40. Hinton DR et al. Novel localization of a G protein, Gz-alpha, in neurons of brain and retina. J. Neurosci 10, 2763–2770 (1990). [PubMed: 2117645]
41. Inoue A et al. Illuminating G-Protein-Coupling Selectivity of GPCRs. Cell 177, 1933–1947.e25 (2019). [PubMed: 31160049]
42. Daaka Y, Luttrell LM & Lefkowitz RJ Switching of the coupling of the beta2-adrenergic receptor to different G proteins by protein kinase A. Nature 390, 88–91 (1997). [PubMed: 9363896]
43. Sandhu M et al. Conformational plasticity of the intracellular cavity of GPCR–G-protein complexes leads to G-protein promiscuity and selectivity. Proc Natl Acad Sci U S A 201820944 (2019) doi:10.1073/pnas.1820944116.
44. Okashah N et al. Variable G protein determinants of GPCR coupling selectivity. Proc Natl Acad Sci U S A 116, 12054–12059 (2019). [PubMed: 31142646]
45. Hervé D Identification of a Specific Assembly of the G Protein Golf as a Critical and Regulated Module of Dopamine and Adenosine-Activated cAMP Pathways in the Striatum. Front Neuroanat 5, (2011).
46. Roth BL Molecular pharmacology of metabotropic receptors targeted by neuropsychiatric drugs. Nature Structural & Molecular Biology 26, 535–544 (2019).
47. Roth BL, Irwin JJ & Shoichet BK Discovery of new GPCR ligands to illuminate new biology. Nat Chem Biol 13, 1143–1151 (2017). [PubMed: 29045379]
48. Navidi WC Statistics for engineers and scientists. (McGraw-Hill Higher Education New York, NY, USA, 2008).

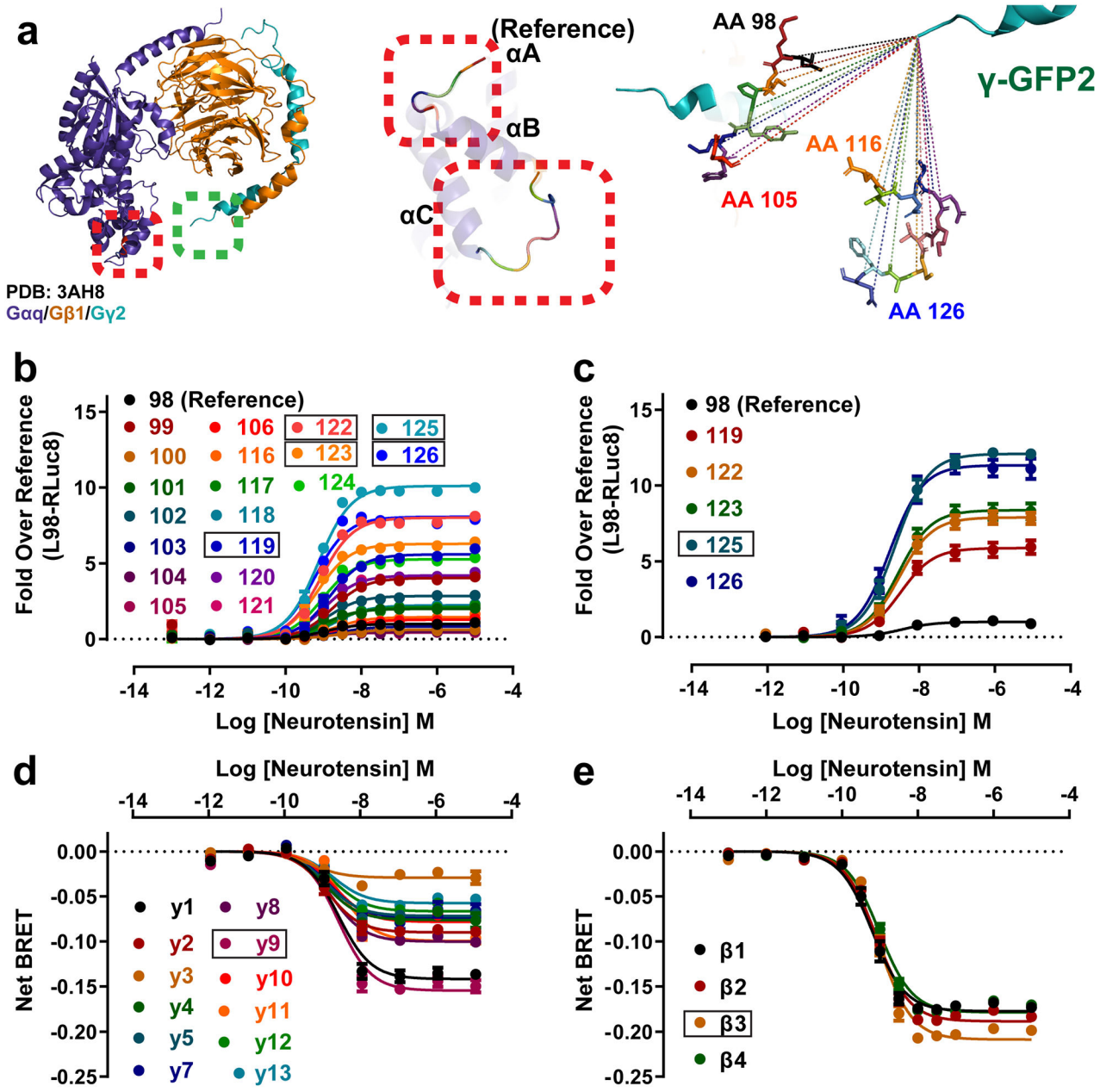

Figure 1. Optimization workflow for the exemplar Gαq biosensor.

(a-c) RLuc8 donor positioning. (a) The inactive Gαq/Gβ1/γ2 crystal structure (PDB 3AH8) defined regions within the alpha-helical domain (red box) in close proximity to the N-terminus of the Gγ-subunit (green box). Twenty Gαq-RLuc8 chimeric proteins were generated between αA-αB and αB-αC helices. (b) Gαq-RLuc8 chimeras were evaluated in duplicate using the prototypic Gαq-coupled NT_1R neurotensin receptor. Performance was evaluated as fold-increase in dynamic range (Net BRET2) relative to the reference construct (insertion of RLuc8 after Lys97 in Gαq was named position 98). (c) The top five RLuc8 positions (119, 122, 123, 125, 126; boxed) were confirmed (N=3) and Gαq(125)-RLuc8 was chosen as the optimal chimeric donor (panel c, boxed). (d) Gγ-GFP2 optimization: the

Gαq(125)-RLuc8 chimera was tested alongside each of 12 N-terminally fused Gγ-GFP2 constructs and a co-precipitated mixture of Gβ1–4 subunits. The Gγ9-GFP2 chimera provided the largest signal (N=3). (e) Gβ optimization: Gαq(125)-RLuc8 and Gγ9-GFP2 were used to screen each of four Gβ subunits (N=3). Stepwise optimization determined that Gαq(125)-RLuc8/Gβ3γ9-GFP2 was the optimal biosensor composition.

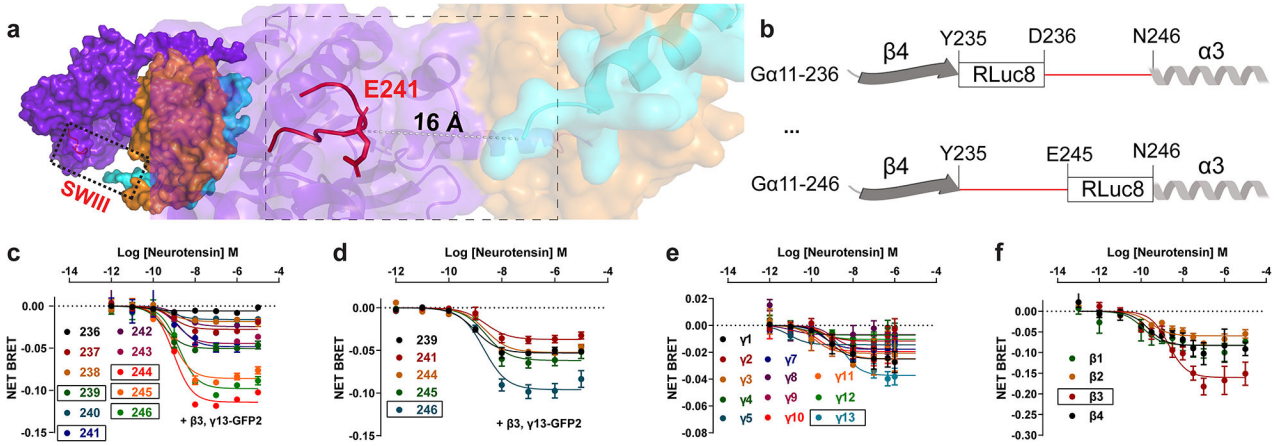

Figure 2. Switch III in the Gα-subunit is a novel region for protein engineering.

(a) For challenging G proteins like Gα11, we identified a new site for RLuc8 insertion located between the β4-strand and α3 helix of the Ras-like domain (denoted Switch III, dashed box). The closest residue in the Gα11 model to the Gγ N-terminus was Glu241 (inset). (b) Schematic delineating the Switch III region and RLuc8 insertion sites for Gα11. (c) Donor optimization results for Gα11 Switch III RLuc8 insertions (N=1, two technical replicates; top 5 positions were 239, 241, 244, 245, 246 (boxed). (d) Gα11(246)-RLuc8 was confirmed as the optimal donor chimera (N=3). (e) Gγ13-GFP2 (boxed) was selected as the optimal BRET2 acceptor (N=3). (f) Gβ3 was selected as the optimal Gβ subunit, yielding Gα11(246)-RLuc8/Gβ3γ13-GFP2 as the final biosensor composition (N=3). Data presented as mean values ± SEM.

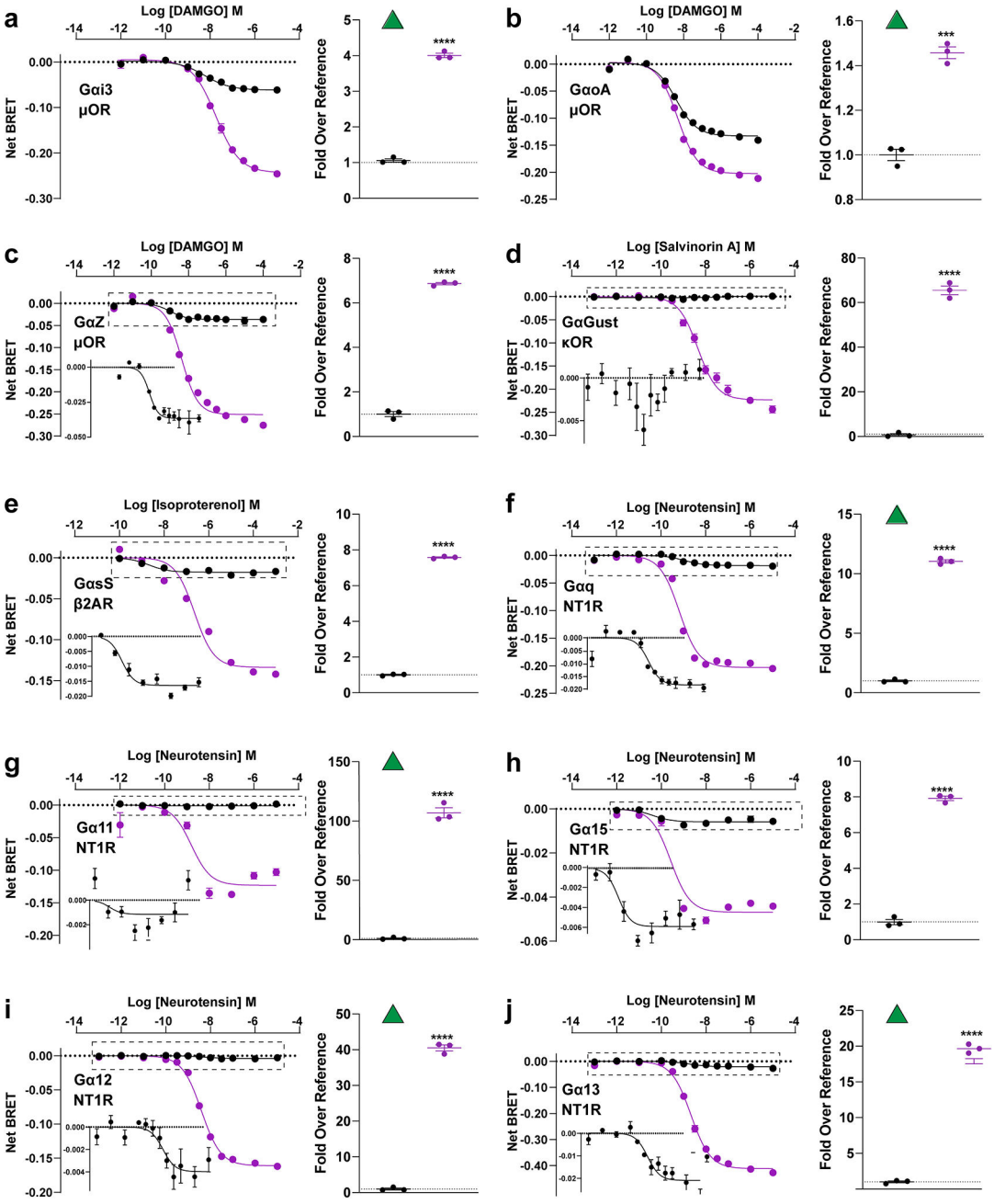

Figure 3. Head-to-head comparisons of TRUPATH biosensors to first-generation BRET2 biosensors.

TRUPATH biosensors are shown in purple and first-generation biosensors are shown in black (published biosensors have green triangles; equivalent RLuc8 positioning was used for previously undisclosed G proteins). Scatter plots show fold difference in amplitude between comparator and TRUPATH biosensors (*two-tailed t-test, $p<0.05$). Additional comparisons are made in Supplemental Figure 18. (a) (Comparator) Gαi3(92)-RLuc8/Gβ1γ2-GFP2 < (TRUPATH) Gαi3(99)-RLuc8/Gβ3γ9-GFP2, $p < 0.0001$. (b) (Comparator) GαoA(92)-RLuc8/Gβ1γ2-GFP2 < (TRUPATH) GαoA(92)-RLuc8/Gβ3γ8-GFP2, $p = 0.0007$ (c) (Comparator) GαZ(92)-RLuc8/Gβ1γ2-GFP2 < (TRUPATH) GαZ(114)-RLuc8/Gβ3γ1-

GFP2, $p < 0.0001$. (d) (Comparator) GαGustducin(92)-RLuc8/Gβ1γ2-GFP2 < (TRUPATH) GαGustducin(117)-RLuc8/Gβ3γ1-GFP2, $p < 0.0001$. (e) (Comparator) GαsS(100)-RLuc8/Gβ1γ1-GFP2 < (TRUPATH) GαsS(123)-RLuc8/Gβ3γ9-GFP2, $p < 0.0001$. (f) (Comparator) Gαq(98)-RLuc8/Gβ1γ1-GFP2 < (TRUPATH) Gαq(125)-RLuc8/Gβ3γ9-GFP2, $p < 0.0001$. (g) (Comparator) Gα11(98)-RLuc8/Gβ1γ1-GFP2 < (TRUPATH) Gα11(246)-RLuc8/Gβ3γ13-GFP2, $p < 0.0001$. (h) (Comparator) Gα15(101)-RLuc8/Gβ1γ2-GFP2 < (TRUPATH) Gα15(245)-RLuc8/Gβ3γ13-GFP2, $p < 0.0001$. (i) (Comparator) Gα12(115)-RLuc8/Gβ1γ2-GFP2 < (TRUPATH) Gα12(134)-RLuc8/Gβ3γ9-GFP2, $p < 0.0001$. (j) (Comparator) Gα13(107)-RLuc8/Gβ1γ2-GFP2 < (TRUPATH) Gα13(126)-RLuc8/Gβ3γ9-GFP2, $p < 0.0001$. Data presented as mean values ± SEM from three biological replicates. Raw values are reported in Supplementary Table 2.

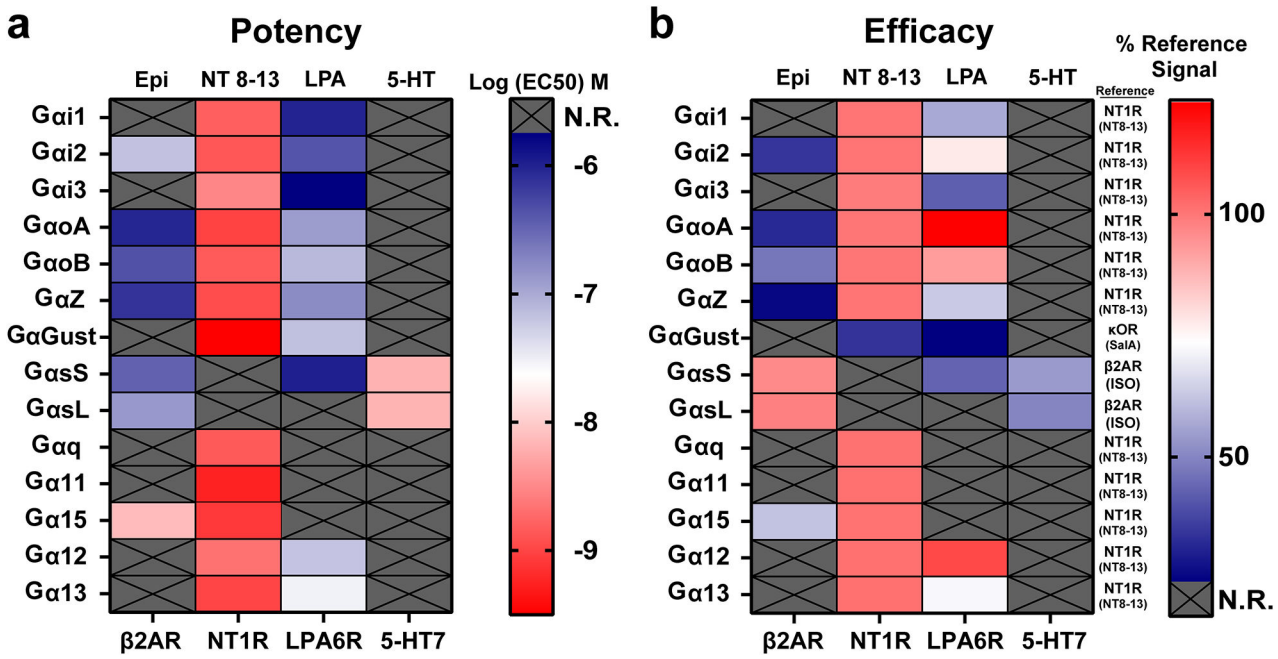

Figure 4. TRUPATH screens of prototypic and understudied GPCRs reveal varying degrees of transducer promiscuity.

Transducerome profiles of endogenous agonists for prototypic receptors (β_2AR β-adrenergic and NT_1R neurotensin) and understudied receptors (LPA_6 LPA and 5-HT_7 serotonin) demonstrate varying degrees of promiscuity. (a) Potency (Log EC_{50}) values are non-uniform across the transducerome for receptor-ligand pairs. (b) Relative amplitude (E_{max} or efficacy) of agonist-induced stimulation of TRUPATH biosensors is frequently non-uniform for a given receptor-ligand pair. Data presented as mean values ± SEM. Heat map values represent mean values. Mean values, standard error, and replicate numbers are reported in Supplementary Dataset 1. Statistically significant differences between efficacies and potencies are reported in Supplementary Datasets 2 and 3, respectively.

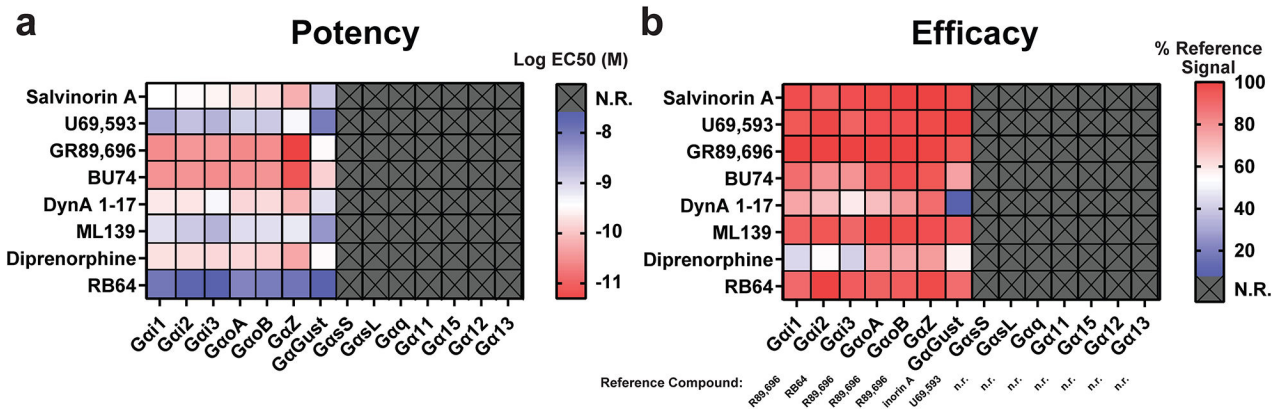

Figure 5. TRUPATH screens of κ-opioid receptor (κOR) agonists reveal unappreciated transducer-selective effects on potency and efficacy.

TRUPATH heatmaps demonstrate how a panel of κOR agonists engage Gαi/o-class transducers with varying potency (a) and efficacy (b). Most ligands exhibit enhanced (GαZ) and diminished (GαGustducin) potencies relative to other G protein transducers. While many ligands activated all transducers with equal efficacy (Salvinorin A, U69,593, GR89,696, ML139, and RB64), others exhibited efficacy bias (BU74, dynorphin A, and diprenorphine). Heatmap colors represent mean Log EC50 and normalized efficacy values. Mean values, standard error, and N are reported in Supplementary Table 4. Statistical analyses of transducer-specific comparisons are reported in Supplementary Datasets 4 (efficacy) and 5 (potency).

Table 1.

Composition of each heterotrimeric BRET2 biosensor in the TRUPATH suite of reagents. Amino Acid (AA) Position number indicates the position in the Gα protein of the first amino acid of the linker flanking the RLuc8 sequence.

Gα	AA Position	Gγ-GFP2	Gβ
i1	91	γ9	β3
i2	91	γ8	β3
i3	99	γ9	β3
oA	92	γ8	β3
oB	92	γ8	β3
Z	114	γ1	β3
Gustducin	117	γ1	β3
sS	123	γ9	β3
sL	137	γ1	β1
Olf	n.d.	n.d.	n.d.
Q	125	γ9	β3
11	246	γ13	β3
14	n.d.	n.d.	n.d.
15	245	γ13	β3
12	134	γ9	β3
13	126	γ9	β3